Published in final edited form as:

Phys Med Biol. 2015 July 7; 60(13): 5103–5121. doi:10.1088/0031-9155/60/13/5103.

An extended analytical approach for diffuse optical imaging

H Erkol[1,2], **F Nouizi**[1], **M B Unlu**[2], and **G Gulsen**[1]

H Erkol: herkol@uci.edu; G Gulsen: ggulsen@uci.edu

[1]Center for Functional Onco Imaging, Department of Radiological Sciences, University of California, Irvine, CA, USA

[2]Department of Physics, Bogazici University, Bebek, 34342, Istanbul, Turkey

Abstract

In this work, we introduce an analytical method to solve the diffusion equation in a cylindrical geometry. This method is based on an integral approach to derive the Green's function for specific boundary conditions. Using our approach, we obtain comprehensive analytical solutions with the Robin boundary condition for diffuse optical imaging in both two and three dimensions. The solutions are expressed in terms of the optical properties of tissue and the amplitude and position of the light source. Our method not only works well inside the tissue but provides very accurate results near the tissue boundaries as well. The results obtained by our method are first compared with those obtained by a conventional analytical method then validated using numerical simulations. Our new analytical method allows not only implementation of any boundary condition for a specific problem but also fast simulation of light propagation making it very suitable for iterative image reconstruction algorithms.

Keywords

Photon propagation; Diffuse optical imaging; Point source

1. Introduction

Diffuse Optical Imaging (DOI) uses near-infrared (NIR) light to determine optical properties of tissue and has a wide range of diagnostic applications from breast cancer to brain imaging [1–6]. In DOI, three dimensional images are obtained using the boundary measurements of NIR light [7–17]. To accomplish this, sources and detectors are placed around tissue and measurements are recorded in reflection or transmission mode. While light propagates, its interaction with biological tissue occurs due to absorption and elastic scattering. Modelling of light propagation in tissue can be achieved accurately by radiative transport equation (RTE) [18]. However, photon transport in turbid medium is generally approximated by the diffusion equation because the RTE is very hard to solve and scattering in tissue is remarkably larger compared to the absorption [19–27]. Photon density throughout the region can be obtained by utilizing analytical, Monte Carlo and numerical methods (such as the Finite Element Method and the Finite Difference Method) [21, 28, 29]. Analytical and

PACS numbers: 87.57.-s,42.50.Ct

Monte Carlo methods yield considerably accurate results compared to numerical methods. Furthermore, analytic methods provide the fastest computational time.

Solving diffusion equation analytically is generally a challenging task. Nevertheless, analytical solutions have been presented for some definite geometries such as spherical or cylindrical as well as sufficiently large or infinite slabs [20–27, 30–39]. In addition, photon propagation, which is obtained by solving the diffusion equation, has also been widely studied for homogeneous sub-layers since some imaging techniques model tissue as a layered structure [24, 34, 36, 40–52]. However, since analytical solutions for irregular geometries have not been obtained, numerical approximation methods such as the Finite Element Method (FEM) and the Finite Difference Method (FDM) are used [21, 22].

Up to date, the Green's function approach has been mainly used to solve the diffusion equation in regular geometries [23, 25]. For example, Arridge *et al* [25] obtained solutions for an infinite cylinder in which an infinitely long line source is placed. They also derived solutions of the diffusion equation for a point source utilizing the Green's function technique in various regular geometries. Furthermore, Sikora *et al* [43] used a series expansion approach to solve the diffusion equation for concentric spheres. In another work, Kienle *et al* [44] obtained continuous wave (cw), frequency and time domain solutions for the diffusion equation via the Green's function method with the extrapolated boundary conditions for a multiple layered finite cylinder. Moreover, Zhang *et al* [38] presented a cw solution for a point source utilizing the extrapolated boundary conditions in cylindrical coordinates. In addition to those, Liemert and Kienle obtained detailed solutions for the diffusion equation in a homogeneous turbid medium with a point source using various integral transformations [37].

In this paper, we obtain both two and three dimensional solutions for the diffusion equation analytically considering steady state (cw) case in a cylindrical medium. Here the light source is modeled by the Dirac δ function with a given strength. We present an integral approach to derive the Green's function for the Robin boundary condition. Our method is indeed very flexible allowing implementation of any boundary condition (i.e. not limited with the Robin boundary condition). Our approach can also be applied to other regular geometries such as spherical. The main motivation of our study is to obtain solutions for the diffusion equation at the boundary making our method very suitable for DOI of homogeneous or nearly homogeneous media. To be able to validate our method, we first compare it with the analytical method presented by Arridge *et al* [25]. Since Arridge *et al* [25] utilize known Green's function of the infinite medium with the zero boundary condition, it corresponds to a special case for our solution. In addition, we compare our results with the solutions obtained by the finite element method in both two and three dimensions.

2. Theoretical method

The photon propagation in tissue is described by the time dependent diffusion equation in time domain [19, 53]

$$\frac{\partial\Phi(\mathbf{r},t)}{c\partial t}+\mu_a\Phi(\mathbf{r},t)-\nabla\cdot[D\nabla\Phi(\mathbf{r},t)]=S(\mathbf{r},t) \quad (1)$$

where Φ, c, D, μ_a, and S represent the photon density, the speed of light, the diffusion coefficient, the absorption coefficient and the source term, respectively. Here, the diffusion coefficient is given as $D(\mathbf{r})=1/(3[\mu_a(\mathbf{r})+\mu_s'(\mathbf{r})])$ where μ_s' is the reduced scattering coefficient. The light source can be considered a point source since it is very small. Hence, the source term can be approximated by the Dirac delta function. As a result of this, we define $S(\boldsymbol{r})=\frac{\Lambda}{c}\delta(\boldsymbol{r},\boldsymbol{r}')$ where $\boldsymbol{r}'$ is the position of the light source and Λ is a dimensionless parameter determining the source strength. For calculational simplicity, we define $\gamma=\frac{\Lambda}{c}$.

For a steady state case (continuous wave), the diffusion equation takes the following form

$$-\nabla^2\Phi(\boldsymbol{r})+\frac{\mu_a}{D}\Phi(\boldsymbol{r})=\frac{\gamma}{D}\delta(\boldsymbol{r},\boldsymbol{r}') \quad (2)$$

where D is taken as constant.

2.1. Two dimensional case

In two dimensional cylindrical coordinates, except for the source position $\mathbf{r}\neq\mathbf{r}_i$, the solution of the diffusion equation is

$$\Phi(r,\theta)=\sum_{m=-\infty}^{\infty}[a_mJ_m(k\,r)+b_mY_m(k\,r)]\,[c_m\cos(m\theta)+d_m\sin(m\theta)] \quad (3)$$

where $k=i\sqrt{\frac{\mu_a}{D}}$ and i is the complex number, J_m and Y_m are the first and second kind Bessel functions, respectively. Here a_m, b_m, c_m, and d_m are the differentiation constants. If the source is placed along the x axis ($\theta=0$), the photon density is symmetric with respect to this axis. In other words, the constant d_m in equation (3) becomes zero so that the angular dependency of the solution comes from $\cos(m\theta)$ term leading to

$$\Phi(r,\theta)=\sum_{m=-\infty}^{\infty}[a_mJ_m(k\,r)+b_mY_m(k\,r)]\cos(m\theta). \quad (4)$$

Now we solve the diffusion equation for a point source using the properties of the Dirac δ function (figure 1). Firstly, we divide the region into two sub-regions according to the position of the source. If $r\leq r_i$, the solution of the radial part consists of only the first kind Bessel function $J_m(kr)$ since the second kind Bessel function goes to infinity at $r=0$. Hence, the solution reduces to

$$\Phi_<(r,\theta)=\sum_{m=-\infty}^{\infty}a_mJ_m(kr)\cos(m\theta) \quad (5)$$

for $r \leq r_i$.

On the other hand, if $R \geq r \geq r_i$, the solution has both of the two radial solutions since the solution is finite in this region. Therefore, the photon density is

$$\Phi_{>}(r,\theta)=\sum_{m=-\infty}^{\infty}[b_m J_m(k\,r)+c_m Y_m(k\,r)]\cos(m\theta) \quad (6)$$

$r \geq r_i$. To relate constants b_m and c_m, we apply the following Robin boundary condition at the boundary surface, $r = R$:

$$\Phi(R,\theta)+2\xi D\frac{\partial\Phi(r,\theta)}{\partial r}|_{r=R}=0 \quad (7)$$

where ξ is a constant corresponding to refractive index mismatched between tissue and its surrounding medium [9, 54, 55].

Now we utilize the properties of the Dirac delta function. The first property is that the solutions of the two regions are equal to each other at the source position. In other words, the expression for the equality of the photon density at $r = r_i$ is

$$\Phi_{<}(r,\theta)|_{r=r_i}=\Phi_{>}(r,\theta)|_{r=r_i}. \quad (8)$$

To represent the sudden change in the derivative of photon density at the source position, let us write solutions into the diffusion equation

$$\sum_{m=-\infty}^{\infty}\{\frac{1}{r}\frac{d}{dr}[r\frac{d}{dr}G_m(kr)]\cos(m\theta)+\frac{1}{r^2}\frac{d^2}{d\theta^2}[\cos(m\theta)]G_m(kr)-\frac{\mu_a}{D}G_m(kr)\cos(m\theta)\}=-\frac{\gamma}{D}\delta(\mathbf{r},\mathbf{r}_i) \quad (9)$$

where $G_m(kr)$ is the following set of Bessel function solutions, $G_m(kr) = \{J_m(kr), Y_m(kr)\}$. Multiplying equation (9) with $r\cos(m'\theta)$ and then integrating between ($r = r_i - \varepsilon$, $\theta = 0$) and ($r = r_i + \varepsilon$, $\theta = 2\pi$) yields

$$\begin{aligned}\sum_{m=-\infty}^{\infty}\int_{r_i-\varepsilon}^{r_i+\varepsilon}[\frac{d}{dr}(r\frac{dG_m(kr)}{dr})]dr\int_0^{2\pi}\cos(m\theta)\cos(m'\theta)d\theta \\ =-\frac{1}{D}\gamma\int_{r_i-\varepsilon}^{r_i+\varepsilon}\int_0^{2\pi}\delta(\mathbf{r},\mathbf{r}_i)\cos(m'\theta)rdrd\theta.\end{aligned} \quad (10)$$

Here notice that except from the first term on the left hand side of equation (9), all the terms go to zero due to the fact that Φ itself is continuous. Next we consider $\varepsilon \to 0^+$ and use the equality of the photon density at the source position given by equation (8). Writing

$$\delta(\mathbf{r},\mathbf{r}_i)=\frac{\delta(r-r_i)\delta(\theta-\theta_i)}{r} \quad (11)$$

and the orthogonality of cosine functions

$$\int_0^{2\pi}\cos(m\theta)\cos(n\theta)d\theta=\pi\delta_{mn} \quad (12)$$

(if m, $n = 0$, equation(12) is 2π) into equation (10) as $\varepsilon \to 0^+$ and using the equality relation of Φ gives the expression for the abrupt change of $\frac{\partial\Phi}{\partial r}$:

$$\frac{dG_m(kr)}{dr}|_{r=r_i+\varepsilon}-\frac{dG_m(kr)}{dr}|_{r=r_i-\varepsilon}=-\frac{\gamma}{\pi D r_i}\cos(m\theta_i). \quad (13)$$

Writing the Robin boundary condition for $\Phi_>$ and substituting $\Phi_>(r, \theta)$ and $\Phi_<(r, \theta)$ into equations (8) and (13) gives

$$b_m J_m(k\,R)+c_m Y_m(k\,R)=-2\xi D[b_m\frac{dJ_m(k\,r)}{dr}+c_m\frac{dY_m(k\,r)}{dr}]|_{r=R}, \quad (14)$$

$$b_m J_m(k\,r_i)+c_m Y_m(k\,r_i)=a_m J_m(k\,r_i) \quad (15)$$

and

$$[b_m\frac{dJ_m(kr)}{dr}+c_m\frac{dY_m(k\,r)}{dr}-a_m\frac{dJ_m(k\,r)}{dr}]|_{r=r_i}=-\frac{\gamma}{\pi D r_i}\cos(m\theta_i). \quad (16)$$

Solving equations (14)–(16) for the differentiation constants a_m, b_m and c_m yields the photon density

$$\Phi(r,\theta)=\sum_{m=-\infty}^{\infty}\begin{cases} a_m J_m(kr)\cos(m\theta) & if \quad r\le r_i \\ (b_m J_m(kr)+c_m Y_m(kr))\cos(m\theta) & if \quad r\ge r_i \end{cases} \quad (17)$$

where $k=i\sqrt{\frac{\mu_a}{D}}$,

$$\begin{gathered} a_m=\frac{\gamma\cos(m\theta_i)}{2D(2Dk\xi RJ_{m-1}(kR)+(R-2Dm\xi)J_m(kR))} \\ \times(J_m(kr_i)(2Dk\xi RY_{m-1}(kR)+(R-2Dm\xi)Y_m(kR)) \\ +Y_m(kr_i)(-2Dk\xi RJ_{m-1}(kR)-(R-2Dm\xi)J_m(kR))), \end{gathered} \quad (18)$$

$$b_m=\gamma R\frac{Dk\xi(Y_{m-1}(kR)-Y_{m+1}(kR))+Y_m(kR)}{2D(2Dk\xi RJ_{m-1}(kR)+(R-2Dm\xi)J_m(kR))}\times J_m(kr_i)\cos(m\theta_i) \quad (19)$$

and

$$c_m=-\frac{\gamma}{2D}J_m(kr_i)\cos(m\theta_i). \quad (20)$$

These two dimensional results can be used for obtaining the photon density around the center when length of the cylindrical volume under investigation is very large.

A special case corresponding to the zero boundary condition can be obtained by setting $\xi = 0$ in the Robin boundary condition. Since this solution has been already presented in detail by Arridge *et al* [25], this approach will allow us to validate our new method. In this case, a_m, b_m and c_m reduce to

$$a_m = \frac{\gamma}{2D}\left[\frac{J_m(kr_i)Y_m(kR)}{J_m(kR)} - Y_m(kr_i)\right]\cos(m\theta_i), \quad (21)$$

$$b_m = \frac{\gamma}{2D}\frac{J_m(kr_i)Y_m(kR)}{J_m(kR)}\cos(m\theta_i), \quad (22)$$

and

$$c_m = -\frac{\gamma}{2D}J_m(kr_i)\cos(m\theta_i), \quad (23)$$

respectively. Now let us use the following relations between the Bessel functions (J_m and Y_m) and the modified Bessel functions (I_m and K_m):

$$I_m(x) = i^{-m}J_m(ix) \quad (24)$$

and

$$K_m(x) = \frac{\pi}{2}i^{m+1}\left[J_m(ix) + iY_m(ix)\right]. \quad (25)$$

Defining $k = i\sqrt{\frac{\mu_a}{D}} \equiv i\alpha$ and then substituting

$$J_m(i\alpha r) = i^m I_m(\alpha r) \quad (26)$$

and

$$Y_m(i\alpha r) = -\frac{2}{\pi i^m}K_m(\alpha r) + i^{m+1}I_m(\alpha r) \quad (27)$$

into equations (21)–(23) yields the photon density for $r > r_i$ given by equation (17)

$$\Phi_>(r,\theta) = \frac{1}{\pi D}\sum_{m=-\infty}^{\infty}\frac{I_m(\alpha r_i)}{I_m(\alpha R)}\left\{K_m(\alpha r)I_m(\alpha R) - K_m(\alpha R)I_m(\alpha r)\right\}\cos(m\theta) \quad (28)$$

by placing the source along the x axis ($\theta_i = 0$). A comprehensive comparison with the solution given by Arridge *et al* [25], can be obtained by transforming the differentiation

constants a_m, b_m and c_m to a'_m, b'_m and c'_m and by using these new constants in equation (17), respectively. The new differentiation constants are $a'_m = a_m/(\sqrt{8\pi}), b'_m = b_m/(\sqrt{8\pi})$ and $c'_m = c_m/(\sqrt{8\pi})$, respectively. In other words, we take the scaled photon density $\Phi_{scaled} = \Phi/(\sqrt{8\pi})$.

Therefore, we obtain the exact solution as the Arridge *et al*'s solution [25]:

$$\Phi_{>}(r,\theta) = \frac{1}{(2\pi)^{\frac{3}{2}} D} \sum_{m=-\infty}^{\infty} \frac{I_m(\alpha r_i)}{I_m(\alpha R)} \{K_m(\alpha r) I_m(\alpha R) - K_m(\alpha R) I_m(\alpha r)\} \cos(m\theta) \quad (29)$$

for $r > r_i$. By interchanging $r \to r_i$, we can also obtain

$$\Phi_{<}(r,\theta) = \frac{1}{(2\pi)^{\frac{3}{2}} D} \sum_{m=-\infty}^{\infty} \frac{I_m(\alpha r)}{I_m(\alpha R)} \{K_m(\alpha r_i) I_m(\alpha R) - K_m(\alpha R) I_m(\alpha r_i)\} \cos(m\theta) \quad (30)$$

for $r < r_i$.

2.2. Three dimensional case

We also present three dimensional results following the similar steps as follows (figure 2). In three dimensional cylindrical coordinates, except for the source position $\mathbf{r} \neq \mathbf{r}_i$, the solution of the diffusion equation is

$$\Phi(r,\theta,z) = \sum_{m=-\infty}^{\infty} \sum_{n=-\infty}^{\infty} [a_{m,n} J_m(\sqrt{k^2+n^2}\, r) + b_{m,n} Y_m(\sqrt{k^2+n^2} r)] \times [c_{m,n} \cos(m\theta) + d_{m,n} \sin(m\theta)]\ [e_{m,n} \cosh(nz) + f_{m,n} \sinh(nz)]. \quad (31)$$

If the source position is in the x axis ($\theta = 0$, $z = 0$), the photon density is symmetric with respect to the x axis. As a result of this, setting the constants $d_{m,n}$ and $f_{m,n}$ in equation (31) to zero provides that the angular and z dependencies of the solution come from $\cos(m\theta)$ and $\cosh(nz)$ terms, respectively. So the solution can be taken as

$$\Phi(r,\theta,z) = \sum_{m=-\infty}^{\infty} \sum_{n=-\infty}^{\infty} [a_{m,n} J_m(\sqrt{k^2+n^2} r) + b_{m,n} Y_m(\sqrt{k^2+n^2} r)] \times \cos(m\theta) \cosh(nz). \quad (32)$$

Now we solve the diffusion equation for a point source using the properties of the Dirac delta function like the two dimensional case. When $r \leq r_i$ and $R \geq r \geq r_i$, the corresponding solutions are

$$\Phi_{<}(r,\theta,z) = \sum_{m=-\infty}^{\infty} \sum_{n=-\infty}^{\infty} a_{m,n} J_m(\sqrt{k^2+n^2}\, r) \cos(m\theta) \cosh(nz) \quad (33)$$

and

$$\Phi_{>}(r,\theta,z)=\sum_{m=-\infty}^{\infty}\sum_{n=-\infty}^{\infty}[b_{m,n}J_m(\sqrt{k^2+n^2}\,r)+c_{m,n}Y_m(\sqrt{k^2+n^2}\,r)]\times\cos(m\theta)\cosh(nz), \quad (34)$$

respectively.

To relate the constants $a_{m,n}$, $b_{m,n}$ and $c_{m,n}$ in equations (33) and (34), we apply the following boundary conditions:

i. the Robin boundary condition at the boundary surface, $r = R$:

$$\Phi(R,\theta,z)+2\xi D\frac{\partial\Phi(r,\theta,z)}{\partial r}|_{r=R}=0 \quad (35)$$

ii. at the ends of the tissue with a length of $2L$, $z = \pm L$:

$$\Phi(r,\theta,\pm L)=0. \quad (36)$$

It is important that the second boundary condition implies that $\cosh(nL) = 0$ or

$$n=i\frac{\pi}{L}(l+\frac{1}{2}) \quad (37)$$

where $l = 0, \pm1, \pm2, \ldots$. In this case, the solution becomes as a function of $\cos(\frac{\pi}{L}(l+\frac{1}{2})z)$ instead of cosine hyperbolic function of z.

Now we use the properties of the Dirac delta function at $r = r_i$ in the expressions for photon density, $\Phi_{<}(r, \theta, z)|_{r=r_i} = \Phi_{>}(r, \theta, z)|_{r=r_i}$, and its derivative. To obtain the expression for the derivative of the photon density, we substitute the radial, angular and z dependent solutions into the three dimensional diffusion equation

$$\begin{aligned}\sum_{m=-\infty}^{\infty}\sum_{l=-\infty}^{\infty}\{&\tfrac{1}{r}\tfrac{d}{dr}[r\tfrac{d}{dr}G_{m,l}(kr)]\cos(m\theta)\cos(\tfrac{\pi}{L}(l+\tfrac{1}{2})z)\\&+\tfrac{1}{r^2}\tfrac{d^2}{d\theta^2}[\cos(m\theta)]G_{m,l}(kr)\cos(\tfrac{\pi}{L}(l+\tfrac{1}{2})z)\\&+\tfrac{d^2}{dz^2}[\cos(\tfrac{\pi}{L}(l+\tfrac{1}{2})z)]G_{m,l}(kr)\cos(m\theta)\\&-\tfrac{\mu_a}{D}G_{m,l}(kr)\cos(m\theta)\cos(\tfrac{\pi}{L}(l+\tfrac{1}{2})z)\}=-\tfrac{\gamma}{D}\delta(\mathbf{r},\mathbf{r}_i)\end{aligned} \quad (38)$$

where $G_{m,l}(kr)$ is the following set of Bessel function solutions,

$G_{m,l}(kr)=\{J_m(\sqrt{k^2-(\frac{\pi}{L}(l+\frac{1}{2}))^2}\,r), Y_m(\sqrt{k^2-(\frac{\pi}{L}(l+\frac{1}{2}))^2}\,r)\}$. Multiplying equation (38) with $r\cos(m'\theta)\cos(\frac{\pi}{L}(l'+\frac{1}{2})z)$ and then integrating between ($r = r_i - \varepsilon$, $\theta = 0$, $z = -L$) and ($r = r_i + \varepsilon$, $\theta = 2\pi$, $z = L$) leads to

$$\begin{aligned}\sum_{m=-\infty}^{\infty}\sum_{l=-\infty}^{\infty}\{\int_{r_i-\varepsilon}^{r_i+\varepsilon}[\tfrac{d}{dr}(r\tfrac{dG_{m,l}(kr)}{dr})]dr\int_0^{2\pi}\cos(m\theta)\cos(m'\theta)d\theta\\ \times\int_{-L}^{L}\cos(\tfrac{\pi}{L}(l+\tfrac{1}{2})z)\cos(\tfrac{\pi}{L}(l'+\tfrac{1}{2})z)dz\}\\ =-\tfrac{1}{D}\gamma\int_{r_i-\varepsilon}^{r_i+\varepsilon}\int_0^{2\pi}\int_{-L}^{L}\cos(m'\theta)\cos(\tfrac{\pi}{L}(l'+\tfrac{1}{2})z)\delta(\mathbf{r},\mathbf{r}_i)rdrd\theta dz.\end{aligned} \quad (39)$$

Here since Φ is continuous, all the terms go to zero except from the first term on the left hand side of equation (38). Next we consider $\varepsilon\to 0^+$ and use

$$\Phi_<(r,\theta,z)|_{r=r_i}=\Phi_>(r,\theta,z)|_{r=r_i}. \quad (40)$$

Substituting $\delta(\mathbf{r},\mathbf{r}_i)=\frac{\delta(r-r_i)\delta(\theta-\theta_i)\delta(z-z_i)}{r}$ and

$$\int_0^{2\pi}\cos(m\theta)\cos(n\theta)d\theta=\begin{cases}2\pi & if \quad m,n=0\\ \pi\delta_{m,n} & if \quad m,n\neq 0\end{cases} \quad (41)$$

as $\varepsilon\to 0^+$ with the equality relation of Φ yields the expression for the $\frac{\partial G_{m,l}}{\partial r}$:

$$\frac{dG_{m,l}(kr)}{dr}|_{r=r_i+\varepsilon}-\frac{dG_{m,l}(kr)}{dr}|_{r=r_i-\varepsilon}=-\frac{\gamma}{\pi DLr_i}\cos(m\theta_i)\cos(\frac{\pi}{L}(l+\frac{1}{2})z_i) \quad (42)$$

Writing the Robin boundary condition for $\Phi_>$ and substituting $\Phi_>(r,\theta,z)$ and $\Phi_<(r,\theta,z)$ into equations (40) and (42) gives

$$\begin{aligned}b_{m,l}J_m(\sqrt{k^2-(\tfrac{\pi}{L}(l+\tfrac{1}{2}))^2}R)+c_{m,l}Y_m(\sqrt{k^2-(\tfrac{\pi}{L}(l+\tfrac{1}{2}))^2}R)\\ +2\xi D[b_{m,l}J_m'(\sqrt{k^2-(\tfrac{\pi}{L}(l+\tfrac{1}{2}))^2}R)+c_{m,l}Y_m'(\sqrt{k^2-(\tfrac{\pi}{L}(l+\tfrac{1}{2}))^2}R)]=0,\end{aligned} \quad (43)$$

$$b_{m,l}J_m(\sqrt{k^2-(\frac{\pi}{L}(l+\frac{1}{2}))^2}\,r_i)+c_{m,l}Y_m(\sqrt{k^2-(\frac{\pi}{L}(l+\frac{1}{2}))^2}\,r_i)=a_{m,l}J_m(\sqrt{k^2-(\frac{\pi}{L}(l+\frac{1}{2}))^2}\,r_i) \quad (44)$$

and

$$\begin{aligned}b_{m,l}J_m'(\sqrt{k^2-(\tfrac{\pi}{L}(l+\tfrac{1}{2}))^2}\,r_i)+c_{m,l}Y_m'(\sqrt{k^2-(\tfrac{\pi}{L}(l+\tfrac{1}{2}))^2}\,r_i)\\ -a_{m,l}J_m'(\sqrt{k^2-(\tfrac{\pi}{L}(l+\tfrac{1}{2}))^2}\,r_i)=-\tfrac{\gamma}{\pi DLr_i}\cos(m\theta_i)\cos(\tfrac{\pi}{L}(l+\tfrac{1}{2})z_i)\end{aligned} \quad (45)$$

where ′ stands for the differentiation with respect to *r*.

Solving equations (43)–(45) for $a_{m,l}$, $b_{m,l}$ and $c_{m,l}$ yields the photon density

$$\Phi(r,\theta,z)=\sum_{m,l=-\infty}^{\infty}\begin{cases} a_{m,l}J_m(\kappa r)\cos(m\theta)\cos(\frac{\pi}{L}(l+\frac{1}{2})z) & if \quad r\le r_i \\ (b_{m,l}J_m(\kappa r)+c_{m,l}Y_m(\kappa r))\cos(m\theta)\cos(\frac{\pi}{L}(l+\frac{1}{2})z) & if \quad r\ge r_i \end{cases} \quad (46)$$

where $\kappa=\sqrt{k^2-(\frac{\pi}{L}(l+\frac{1}{2}))^2}$ for the calculational simplicity and

$$\begin{aligned} a_{m,l}=&\frac{\gamma\cos(m\theta_i)\cos(\frac{\pi}{L}(l+\frac{1}{2})z_i)}{2DL(2D\kappa\xi RJ_{m-1}(\kappa R)+(R-2Dm\xi)J_m(\kappa R))} \\ &\times(J_m(\kappa r_i)(2D\kappa\xi RY_{m-1}(\kappa R)+(R-2Dm\xi)Y_m(\kappa R)) \\ &+Y_m(\kappa r_i)(-2D\kappa\xi RJ_{m-1}(\kappa R)-(R-2Dm\xi)J_m(\kappa R))), \end{aligned} \quad (47)$$

$$b_{m,l}=\gamma R\frac{D\kappa\xi(Y_{m-1}(\kappa R)-Y_{m+1}(\kappa R))+Y_m(\kappa R)}{2DL(2D\kappa\xi RJ_{m-1}(\kappa R)+(R-2Dm\xi)J_m(\kappa R))}\times J_m(\kappa r_i)\cos(m\theta_i)\cos(\frac{\pi}{L}(l+\frac{1}{2})z_i) \quad (48)$$

and

$$c_{m,l}=-\frac{\gamma}{2DL}J_m(\kappa r_i)\cos(m\theta_i)\cos(\frac{\pi}{L}(l+\frac{1}{2})z_i). \quad (49)$$

Similar to the two dimensional case, we also obtain a solution corresponding to the zero boundary condition for the three dimensional case to be able to compare our method with Arridge *et al*'s method and validate it. Setting $\xi = 0$ in the Robin boundary condition, the differentiation constants reduce to

$$a_{m,l}=\frac{\gamma}{2D}[\frac{J_m(\kappa r_i)Y_m(\kappa R)}{J_m(\kappa R)}-Y_m(\kappa r_i)]\cos(m\theta_i)\cos(\frac{\pi}{L}(l+\frac{1}{2})z_i), \quad (50)$$

$$b_{m,l}=\frac{\gamma}{2D}\frac{J_m(\kappa r_i)Y_m(\kappa R)}{J_m(\kappa R)}\cos(m\theta_i)\cos(\frac{\pi}{L}(l+\frac{1}{2})z_i), \quad (51)$$

and

$$c_{m,l}=-\frac{\gamma}{2D}J_m(\kappa r_i)\cos(m\theta_i)\cos(\frac{\pi}{L}(l+\frac{1}{2})z_i), \quad (52)$$

respectively. Now we define $\kappa=\sqrt{k^2-(\frac{\pi}{L}(l+\frac{1}{2}))^2}\equiv i\alpha_l$ for the calculational simplicity. We substitute

$$J_m(i\alpha_l r)=i^m I_m(\alpha_l r) \quad (53)$$

and

$$Y_m(i\alpha_l r) = -\frac{2}{\pi i^m} K_m(\alpha_l r) + i^{m+1} I_m(\alpha_l r) \quad (54)$$

into equations (50)–(52). Next we transform the differentiation constants $a_{m,l}$, $b_{m,l}$ and $c_{m,l}$ to $\frac{a_{m,l}}{\sqrt{8\pi}}$, $\frac{b_{m,l}}{\sqrt{8\pi}}$ and $\frac{c_{m,l}}{\sqrt{8\pi}}$, or equivalently, we take the scaled solution $\Phi_{scaled} = \Phi/(\sqrt{8\pi})$. Therefore, the solutions are

$$\Phi_>(r,\theta,z) = \frac{1}{\pi(2\pi)^{1/2} DL} \sum_{n=-\infty}^{\infty} \sum_{l=-\infty}^{\infty} \frac{I_m(\alpha_l r_i)}{I_m(\alpha_l R)} \{K_m(\alpha_l r) I_m(\alpha_l R) - K_m(\alpha_l R) I_m(\alpha_l r)\} \times \cos(m\theta) \cos\left(\frac{\pi}{L}\left(l + \frac{1}{2}\right) z\right) \quad (55)$$

and

$$\Phi_<(r,\theta,z) = \frac{1}{\pi(2\pi)^{1/2} DL} \sum_{n=-\infty}^{\infty} \sum_{l=-\infty}^{\infty} \frac{I_m(\alpha_l r)}{I_m(\alpha_l R)} \{K_m(\alpha_l r_i) I_m(\alpha_l R) - K_m(\alpha_l R) I_m(\alpha_l r_i)\} \times \cos(m\theta) \cos\left(\frac{\pi}{L}\left(l + \frac{1}{2}\right) z\right) \quad (56)$$

for $r > r_i$ and $r < r_i$, respectively. Therefore, we obtain a similar solution to the Arridge *et al*'s solution apart from the different boundary condition that Arridge *et al* used [25].

3. Numerical application and validation

To validate our theoretical method in two and three dimensions, we perform numerical calculations and simulations using other methods. For 2D case, our results are compared with another analytical method while simulations obtained by using Finite Element Method are used to validate both 2D and 3D cases. These simulations are obtained by solving the diffusion equation numerically with the Comsol Multiphysics solver [12, 56– 58].

For all calculations, we set the absorbtion coefficient (μ_a), the reduced scattering coefficient (μ_s') and the refractive index (n) to 0.0132 mm^{-1}, 0.5 mm^{-1} and 1.4, respectively. The diameter and length of the cylindrical tissue are R = 25 mm and $2L$ = 100 mm, respectively.

In 2D case, we first compare our approach with the analytic method presented by Arridge *et al* [25]. We obtain the photon density distribution along the *xy* plane and its profile in terms of the radial position for a tissue domain with a radius of R = 12.5 mm. In this case, we take the source position and its strength $\mathbf{r}_i = (r_i = R/2, \theta_i = 0)$ along the x axis and γ = 100 s/mm, respectively. Figures 3 and 4 exhibit the photon density distribution and its profile along the x-axis, respectively. In figure 4, we use the Arridge *et al*'s [25] results which are normalized according to ours. Figure 4 also shows that the results differ slightly in the vicinity of the boundary, which arises from the utilization of the different boundary conditions. In fact, Arridge *et al* [25] use the Dirichlet boundary condition ($\Phi(R, \theta) = 0$) whereas we use the Robin boundary condition. The results for these two methods are in good agreement inside the medium. To demonstrate the validation of our method in the whole tissue domain, we next locate the source near the tissue center. We obtain the photon density distribution in the *xy* plane and present it in figure 5 by locating the source at $\mathbf{r}_i = (r_i = 0.1R, \theta_i = 0)$ with a strength of γ = 100 s/mm. The photon density profile is obtained along the *x* axis ($\theta = 0$)

both analytically and numerically based on the finite element method in figure 6. The profiles for these methods are in good agrement. The only slight difference between them is that the photon density obtained by our approach is a little bit higher than the one obtained by the finite element method. This small difference results from the approximation that the finite element method uses and its lack of accuracy near the source position. Secondly, we place the source near the tissue boundary and perform similar calculations. For this case, we take the strength and position of the source $\gamma = 100$ s/mm and $\mathbf{r}_i = (r_i = R - 1/\mu_s', \theta_i = 0)$, respectively. We obtain the photon density distribution in the xy plane as shown in figure 7. Figure 8 shows the photon density profiles along the x direction for both methods. We observe that these profiles obtained by our analytical and numerical methods match closely, like the former case. These results confirm that our method works well for both near the center and in the vicinity of the boundary.

For practical DOI applications, we also extend the method in three dimensions for a finitely long cylindrical geometry. Figure 9 shows the schematic of this case in which photon density distribution is obtained by the finite element method and superimposed for illustration purpose. Similar to the two dimensional case, we again solve the diffusion equation analytically using our approach and numerically with the FEM method. In practice, sources and detectors are placed at the boundary for DOI. However, the source is placed at one scattering path length under the surface due to the diffusion equation approximation. For this reason, we place the source at ($r_i = R - 1/\mu_s'$, $\theta_i = 0$, $z_i = 0$). Here the diameter and the length of the cylindrical tissue are chosen as R=25 mm and $2L = 100$ mm, respectively. In the calculations, 16 detectors are equispatially placed around the tissue boundary (figure 9). In other words, each detector makes an angle $2d\pi/360°$ with the x axis where d is the detector number ranging from 1 to 16. The photon flux, $\Lambda = \Phi/(2\xi)$ is calculated both analytically using our approach and numerically based on the synthetic detector measurements. We obtain the logarithm of the photon flux at various z positions ($z = 0, 3, 6$ mm) and present our results in figure 10. The comparison of these two methods shows that the results are in very good agrement.

4. Discussion and conclusion

In this contribution, we present an analytical approach to solve the diffusion equation using an integral method and the Dirac δ light source with a given strength in two and three dimensions. These solutions are expressed for a homogeneous cylindrical geometry. Liemert and Kienle [37] also solved the diffusion equation for a homogeneous turbid cylinder with a point source using various integral transformations (Hankel, Laplace, Fourier, sine and cosine integral transforms) with an extrapolated boundary condition. Different from Liemert and Kienle's work, we use an integral method to solve the diffusion equation by obtaining a particular Green's function. It is also important to notice that we utilize the Robin boundary condition. Although we utilize the Robin boundary condition, which is adequate for imaging of biological tissue, our approach is indeed flexible allowing for implementation of any boundary condition. In fact, our method takes advantage of the mathematical properties of the Dirac δ source and the symmetry of the geometry.

Our results mainly consist of comprehensive series solutions. In our approach, it is not necessary to calculate infinite number of roots for the Bessel functions arising from the Robin boundary condition. Actually, we use the Robin boundary condition to relate differentiation constants to each other to obtain the solution. The results obtained by our method and those obtained by the analytical method given by Arridge *et al* [25] turn out to be in good agreement inside the medium. On the other hand, the results differ slightly when approaching the tissue boundary because Arridge *et al* [25] use the zero boundary condition while we use the Robin boundary condition. This explains why the solution of Arridge *et al* becomes zero and our solution tends to a finite value at the boundary. We also show that setting parameter ξ in the Robin boundary condition to zero (corresponding to the zero boundary condition), our normalized results reduce to the Arridge *et al*'s results [25]. To further validate our method, we also solve the diffusion equation numerically using the finite element method. Indeed, the results obtained by these two methods are in good agreement. Moreover, our method gives more accurate solution at the medium boundary as well as near the source position. In fact, this is important since the DOI measurements are performed at the surface.

Another advantage of our method is that it reduces computational time compared to numerical methods such as the finite element method and the finite difference method. Actually, our method does not require any complex calculations and the solutions are simply given by equation (17) and equation (46) for two and three dimensions, respectively. At first, it seems like we have to compute two summations with infinite number of terms. As a matter of fact, when we expand the solution, we see that after some limit, the contribution coming from the higher order terms approaches to zero. In fact, we observe that the first 50 terms for l and m are sufficient for an accurate solution. Modeling of photon transport in tissue is important for imaging applications. Image reconstruction in DOI is a very long iterative process since the forward problem has to be solved at each iteration during the image reconstruction. This is one of the barriers that hinders translation of DOI to clinical settings. Thus, combining our technique with a conventional numerical method would accelerate the image reconstruction process. In fact, the reconstruction process can be considerably accelerated by implementing our analytical solution to the weight matrices [59] when imaging highly homogeneous organs such as breast.

Acknowledgments

We would like to thank all the reviewers for their instructive and valuable comments. This research is supported by National Institutes of Health (NIH) grants R01EB008716, R21EB013387 and P30CA062203, TUBITAK Grant 2219, Bogazici University Research funding Grant No. BAP 7126 and TUBITAK Grant No. 112T253.

References

1. Tromberg BJ, Cerussi A, Shah N, Compton M, Durkin A, Hsiang D, Butler J, Mehta R. Breast Cancer Res. 2005; 7(6):279. [PubMed: 16457705]
2. Tromberg BJ. Acad Radiol. 2005; 12(8):923. [PubMed: 16087089]
3. Tromberg BJ, Pogue BW, Paulsen KD, Yodh AG, Boas DA, Cerussi AE. Med Phys. 2008; 35(6): 2443. [PubMed: 18649477]
4. Gibson AP, Hebden JC, Arridge SR. Phys Med Biol. 2005; 50(4):R1. [PubMed: 15773619]

5. Cerussi A, Shah N, Hsiang D, Durkin A, Butler J, Tromberg BJ. J Biomed Opt. 2006; 11(4):044005. [PubMed: 16965162]
6. Cerussi A, Hsiang D, Shah N, Mehta R, Durkin A, Butler J, Tromberg BJ. Proc Natl Acad Sci. 2007; 104(10):4014. [PubMed: 17360469]
7. Pogue BW, Zhu H, Nwaigwe C, McBride TO, Osterberg UL, Paulsen KD, Dunn JF. Adv Exp Med Biol. 2003; 530:215. [PubMed: 14562719]
8. Pogue BW. Acad Radiol. 2006; 13(1):1. [PubMed: 16399027]
9. Arridge SR. Inverse Probl. 1999; 15:R41.
10. Hielscher AH, Bluestone AY, Abdoulaev GS, Klose AD, Lasker J, Stewart M, Netz U, Beuthan J. Dis Markers. 2002; 18(5–6):313. [PubMed: 14646043]
11. Unlu MB, Gulsen G. Appl Opt. 2008; 47(6):799. [PubMed: 18288229]
12. Unlu MB, Birgul O, Gulsen G. Phys Med Biol. 2008; 53(12):3189. [PubMed: 18506072]
13. Unlu MB, Lin Y, Birgul O, Nalcioglu O, Gulsen G. J Biomed Opt. 2008; 13:060501. [PubMed: 19123642]
14. Dehghani H, Delpy DT, Arridge SR. Phys Med Biol. 1999; 44(12):2897. [PubMed: 10616143]
15. Dehghani H, Arridge SR, Schweiger M, Delpy DT. J Opt Soc Am A. 2000; 17(9):1659.
16. Valim N, Brock J, Leeser M, Niedre MJ. Phys Med Biol. 2013; 58(2):335. [PubMed: 23257349]
17. Valim N, Brock J, Niedre MJ. J Biomed Opt. 2010; 15(6):065006. [PubMed: 21198170]
18. Darne C, Lu Y, Sevick-Muraca EM. Phys Med Biol. 2014; 59(1):R1. [PubMed: 24334634]
19. Wang, LV.; Wu, H. Biomedical Optics: Principles and Imaging. Wiley; New Jersey: 2007. p. 97
20. Patterson MS, Madsen SJ. IEEE MTT-SDigest. 1991; 2:905.
21. Arridge SR, Schweiger M, Hiraoka M, Delpy DT. Med Phys. 1993; 20:299. [PubMed: 8497214]
22. Schweiger M, Arridge SR, Delpy DT. J Mat Imaging Vis. 1993; 3:263.
23. Patterson MS. Appl Opt. 1989; 28:2331. [PubMed: 20555520]
24. Schmitt JM, Zhou GX, Walker EC, Wall RT. J Opt Soc Am A. 1990; 7:2141. [PubMed: 2254803]
25. Arridge SR, Cope M, Delpy DT. Phys Med Biol. 1992; 37:1531. [PubMed: 1631197]
26. Farrel TJ, Patterson MS, Wilson BC. Med Phys. 1992; 19:879–888. [PubMed: 1518476]
27. Boas DA, O'leary MA, Chances B, Yodh AG. Proc Natl Acad Sci. 1994; 91:4887. [PubMed: 8197151]
28. Das RK, Li Z, Perera H, Williamson JF. Phys Med Biol. 1996; 41:995. [PubMed: 8794480]
29. Flock ST, Patterson MS, Wilson BC, Wyman DR. IEEE Trans Biomed Eng. 1989; 36:1162. [PubMed: 2606490]
30. Walker SA, Boas DA, Gratton E. Appl Opt. 1998; 37:1935. [PubMed: 18273113]
31. Pogue BW, Patterson MS. Phys Med Biol. 1994; 39:1157. [PubMed: 15552104]
32. Contini D, Martelli F, Zaccanti G. Appl Opt. 1997; 36:4587. [PubMed: 18259254]
33. Kienle A, Patterson MS. J Opt Soc Am A. 1997; 14:246.
34. Martelli F, Sassaroli A, Yamada Y, Zaccanti G. J Opt Soc Am A. 2002; 19:71.
35. Kienle A. J Opt Soc Am A. 2005; 22:1883.
36. Martelli F, Sassaroli A, Bianco SD, Zaccanti G. Phys Med Biol. 2007; 52:2827. [PubMed: 17473354]
37. Liemert A, Kienle A. Opt Express. 2010; 18:9456. [PubMed: 20588792]
38. Zhang A, Piao D, Bunting CF, Pogue BW. J Opt Soc Am A. 2010; 27:648.
39. Cong W, Wang LV, Wang G. Biomed Eng Online. 2004; 3:1. [PubMed: 14746653]
40. Takatani S, Graham MD. IEEE Trans Biomed Eng. 1979; 26:656. [PubMed: 544437]
41. Liemert A, Kienle A. Opt Express. 2010; 18:9266. [PubMed: 20588774]
42. Dayan I, Havlina S, Weissb GH. J Mod Opt. 1992; 39:1567.
43. Sikora J, Zacharopoulos A, Douiri A, Schweiger M, Horesh L, Arridge SR, Ripoll J. Phys Med Biol. 2006; 51:497. [PubMed: 16424578]
44. Liemert A, Kienle A. J Biomed Opt. 2010; 15:025002. [PubMed: 20459243]

45. Okada E, Firbank M, Schwiger M, Arridge SR, Cope M, Delpy DT. Appl Opt. 1997; 36:21. [PubMed: 18250644]
46. Svaasand LO, Spott T, Fishkin JB, Pham T, Tromberg BJ, Berns MW. Phys Med Biol. 1999; 44:801. [PubMed: 10211811]
47. Kienle A, Glanzmann T. Phys Med Biol. 1999; 44:2689. [PubMed: 10588278]
48. Pogue BW, McBride TO, Osterberg UL, Paulsen KD. Opt Express. 1999; 4:270. [PubMed: 19396284]
49. Dehghani H, Delpy DT. Appl Opt. 2000; 39:4721. [PubMed: 18350064]
50. Dehghani H, Brooksby BA, Pogue PW, Paulsen KD. Appl Opt. 2005; 44:1870. [PubMed: 15813524]
51. Yalavarthy PK, Dehghani H, Pogue BW, Paulsen KD. Opt Express. 2006; 14
52. Schweiger M, Arridge SR. Med Phys. 1997; 24:895. [PubMed: 9198025]
53. Nouizi F, Torregrossa M, Chabrier R, Poulet P. Opt Express. 2011; 19:12843. [PubMed: 21716527]
54. Gao H, Zhao H, Cong W, Wang G. Biomed Opt Express. 2010; 1:1259. [PubMed: 21258547]
55. Liu K, Tiana J, Lu Y, Qin C, Yang X, Zhu S, Zhang X. Opt Express. 2010; 18(4):3732. [PubMed: 20389383]
56. Nouizi F, Chabrier R, Torregrossa M, Poulet P. Proc SPIE. 2009; 7369:73690C.
57. Lin Y, Gao H, Thayer D, Luk AL, Gulsen G. Phys Med Biol. 2003; 58:3551. [PubMed: 23640084]
58. Erkol H, Unlu MB. Appl Opt. 2013; 52:4933. [PubMed: 23852209]
59. Wang D, Song X, Bai J. Opt Express. 2007; 15:9722. [PubMed: 19547322]

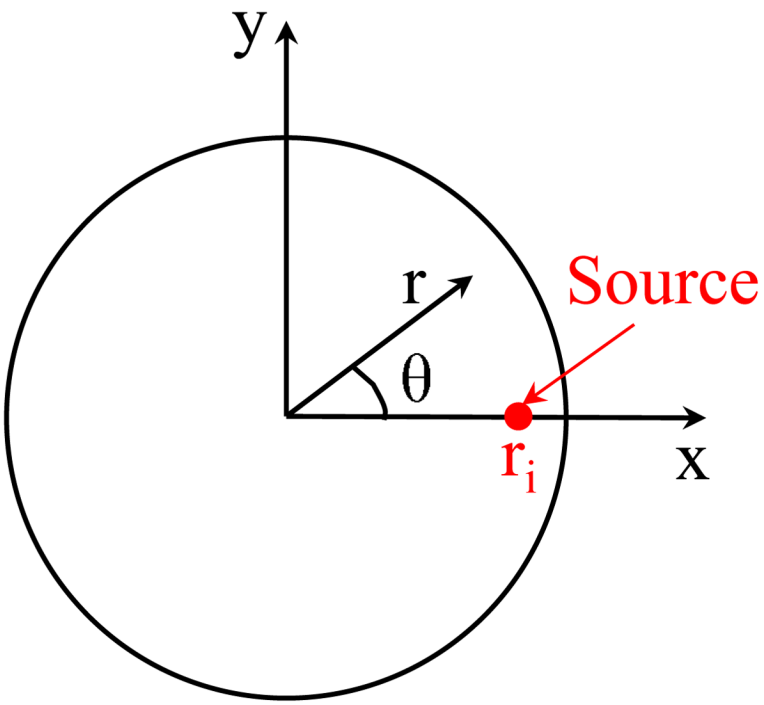

Figure 1.
The schematic showing the geometry of a homogeneous medium with a δ function source in two dimensions.

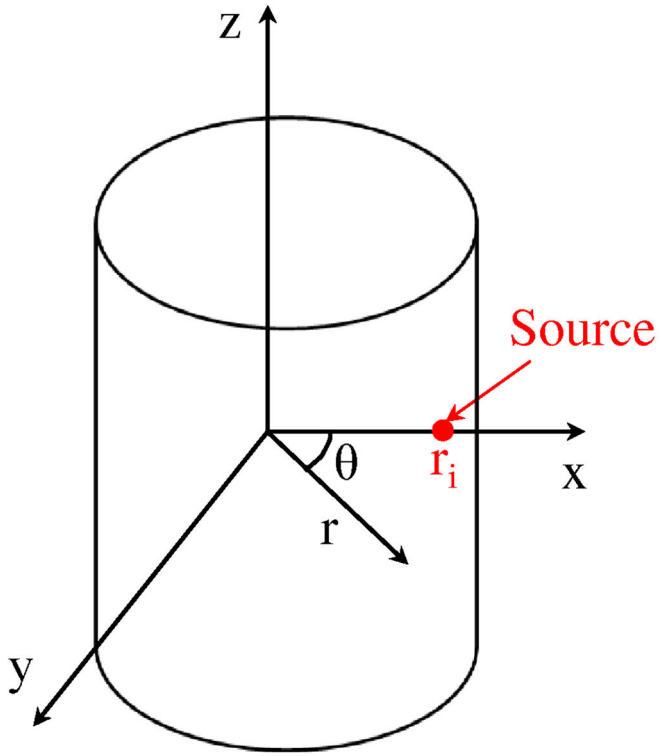

Figure 2.
The schematic showing the geometry of a homogeneous medium with a δ function source in three dimensions.

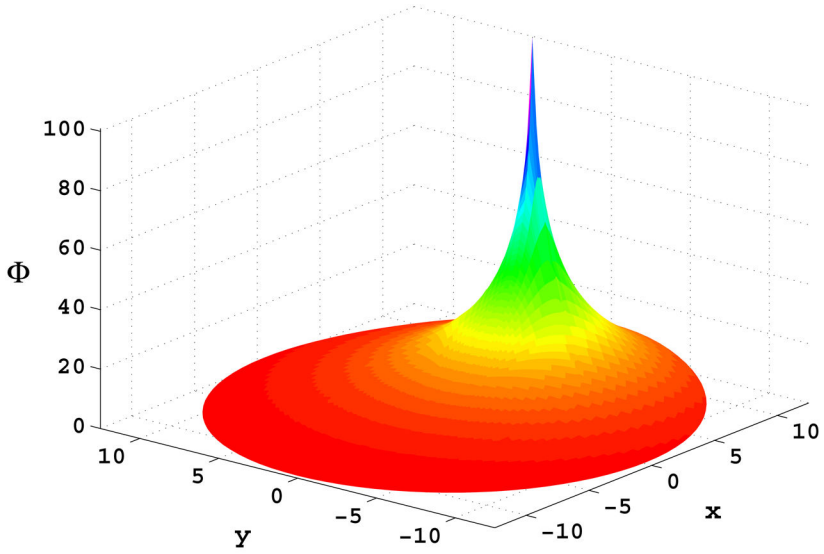

Figure 3.

Photon density Φ (in units of s.mm^{-2}) vs. x (mm) and y (mm) for a source of a strength γ = 100 s/mm and located at $r_i = (x_i = R/2, y_i = 0)$.

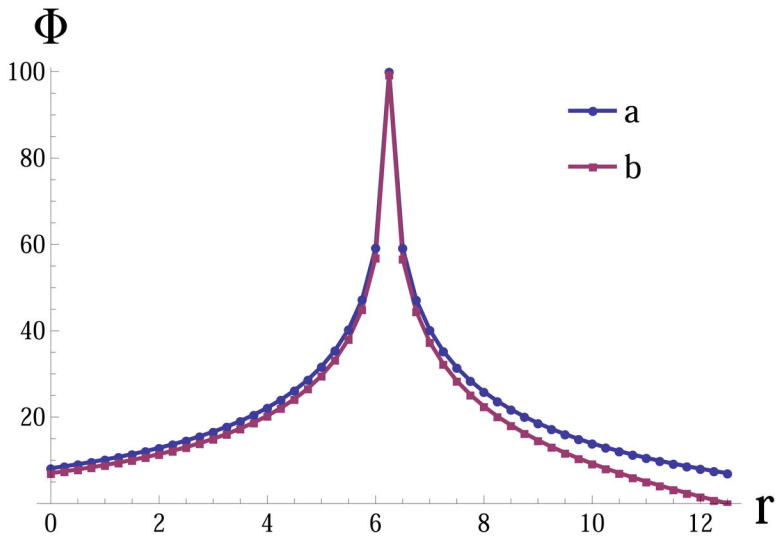

Figure 4.

Photon density Φ (in units of s.mm^{-2}) vs. radial distance r (mm) at $\theta = 0$ for a point source of a strength $\gamma = 100$ s/mm described by $\delta(r_i = R/2, \theta_i = 0)$. Here a (circle) shows our work with the Robin boundary condition and b (square) shows the Arridge's work with the Dirichlet boundary condition for a circular domain of radius $R = 12.5$mm.

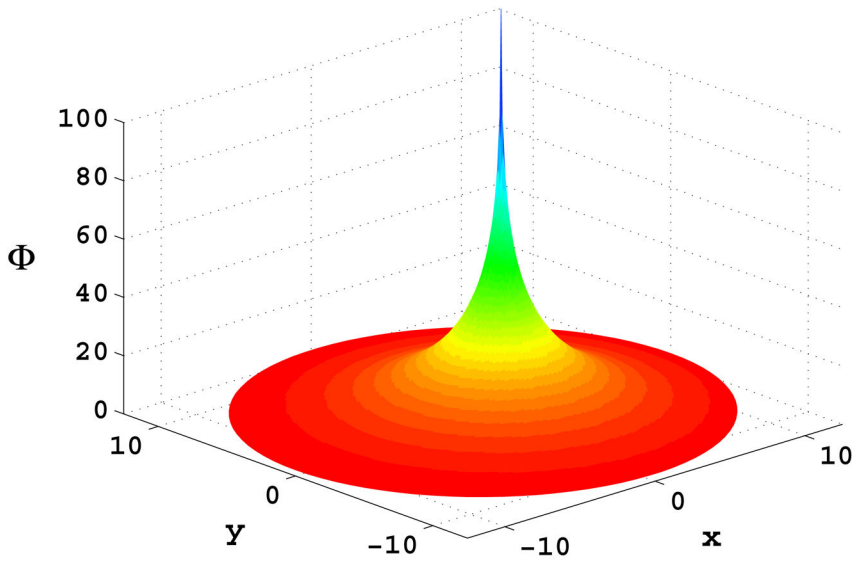

Figure 5.

Photon density Φ (in units of s.mm^{-2}) vs. x (mm) and y (mm) for a source of a strength $\gamma =$ 100 s/mm near the center, $r_i = (x_i = 0.1R, y_i = 0)$.

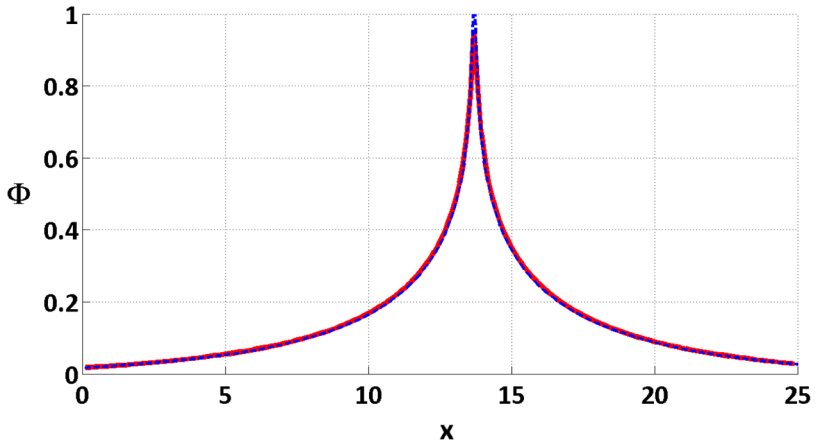

Figure 6.

The normalized photon density profile Φ (in units of s.mm^{-2}) vs. *x* (mm) for a source near the center. The dash line (blue) shows the analytical approach while the solid line (red) shows the finite element method.

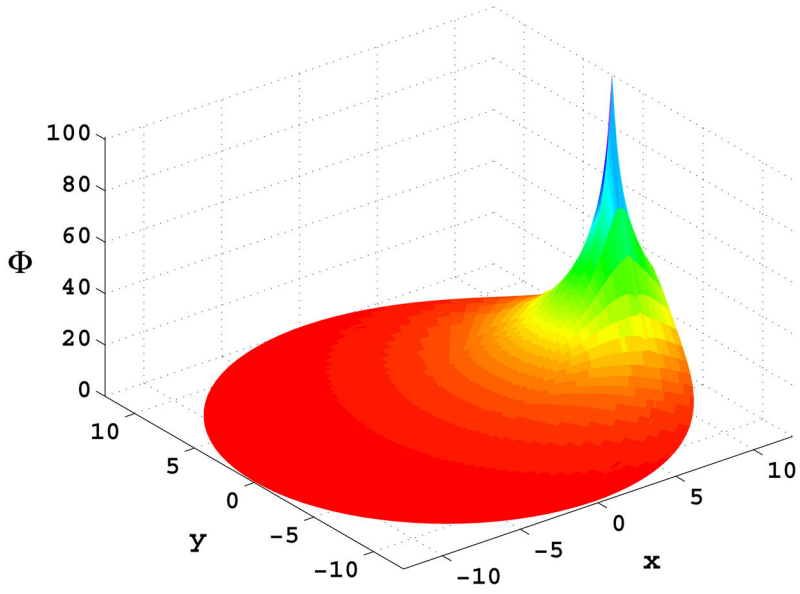

Figure 7.

Photon density Φ (in units of s.mm^{-2}) vs. x (mm) and y (mm) for a source of a strength $\gamma =$ 100 s/mm near the boundary, $r_i=(x_i=R-\frac{1}{\mu_s'}, y_i=0)$.

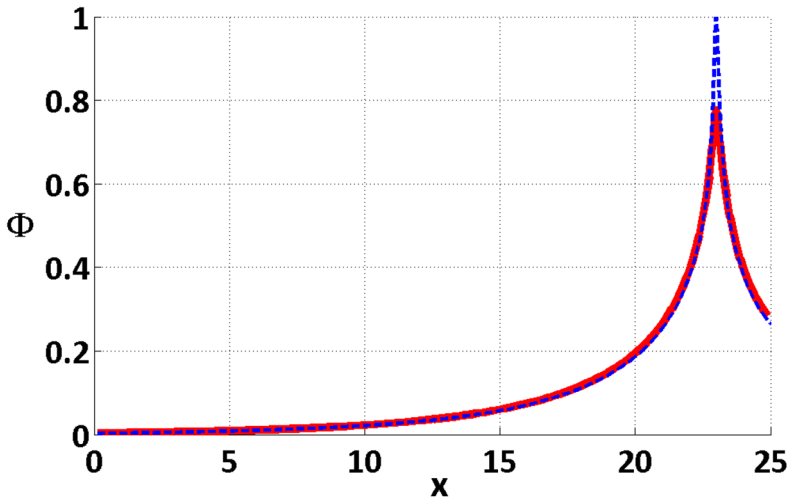

Figure 8.

The normalized photon density profile Φ (in units of s.mm^{-2}) vs. x (mm) for a source near the boundary. The dash line (blue) shows the analytical approach while the solid line (red) shows the finite element method.

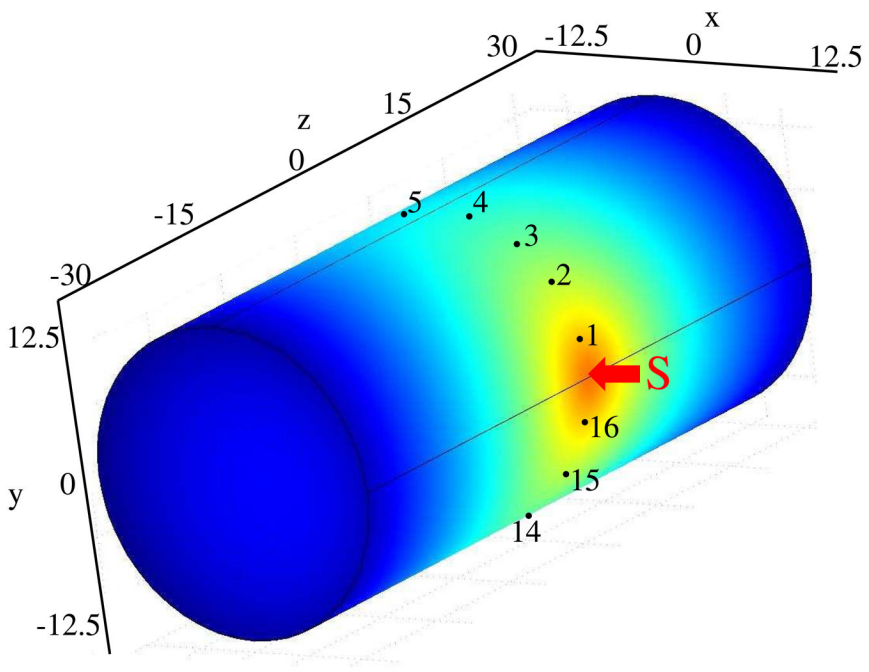

Figure 9.

The schematic of the three dimensional case where numbers and S represent the detectors and the source, respectively. The photon density distribution is obtained by the finite element method and superimposed for illustration purpose.

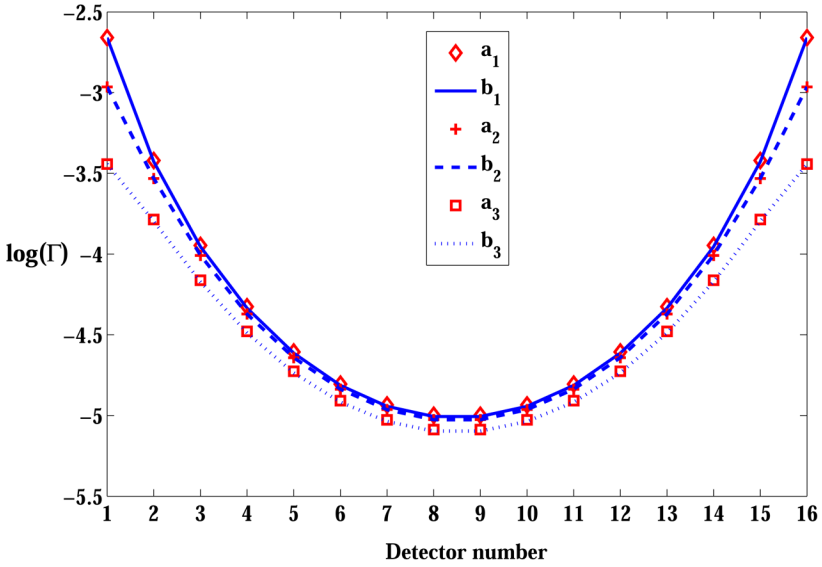

Figure 10.

Logarithm of the photon flux log(Λ) vs. detector number at various $z = 0, 3, 6$ mm positions for a source near the boundary, $r_i=(x_i=R-1/\mu_s', y_i=0)$. Here a_i and b_i represent the analytical results and the numerical results obtained by our approach and the finite element method, respectively. Subindex $i = 1, 2, 3$ corresponds to $z = 0, 3, 6$ mm, respectively.